JOURNAL OF PROPULSION AND POWER
Vol. 18, No. 3, May–June 2002

# High-Pressure Steam Flow in Turbine Bypass Valve System Part 2: Pipe Flow

R. S. Amano,* G. R. Draxler,† and J. M. Golembiewski‡
*University of Wisconsin—Milwaukee, Milwaukee, Wisconsin 53201*

**The main goal of this study is to investigate the evaporation process of a coolant (water droplets), which is injected through spray nozzles mounted on a steam turbine bypass pipeline in a cogenerator system. The study includes several important factors: 1) the effects of four elbows on the flow pattern and evaporation process of the water particles, 2) heat transfer that affects the steam temperature and also the evaporation rates, and 3) the effects of a perforated plate on the flow pattern and evaporation process. The first goal of this study is to investigate whether or not the existence of elbows in the pipeline will enhance the evaporation process of cooling water droplets. Two effects have been observed so far: one is that the generation of turbulence increases in the core of the elbow, which results in a higher heat-transfer rate between particles and steam, and the other is that water particles are forced to impinge onto the outer side of the pipe wall in the elbow due to the centrifugal inertia force of the flow in the curvature path. The second goal is to carefully study the heat-transfer effects of three different modes, i.e., the heat exchange between the steam and the water particles, the heat transfer of flow to the wall caused by turbulence convection, and the conjugate heat transfer by means of heat conduction through the pipe wall and insulation materials. The last goal of the research is to investigate the effect of the insertion of a perforated plate downstream from the cooling water spray nozzles. A detailed analysis was conducted by microscopically modeling the flow through each hole of the perforated plate. Modeling of the high-pressure turbulent steam flow was based on a nonstaggered finite volume method in three-dimensional, turbulent, compressible, and two-phase dispersed flow formulations. The investigation of the structure of liquid spray jets during the transition into the gaseous phase was accomplished by developing a physical model of a particle tracking technique to investigate evaporation processes of the liquid droplets in a highly turbulent flow. Computations were performed by separating the entire pipeline system into four sections, each of which was generated in a three-dimensional grid system for more efficient computations by maintaining a sufficiently large number of meshes for each section. Flow calculations were made in each region separately by patching the end conditions from one pipe to the inlet conditions of the next one. Through this research numerous data have been acquired and analyzed for heat-transfer mechanisms of the evaporation of the water droplets in the pipeline system along with the cooling of the steam flow. The results of the computations were verified by comparing them with theoretical models and were shown to be quite reliable.**

## Nomenclature

| | | |
|---|---|---|
| $A$ | = | area |
| $C_b$ | = | vaporization constant |
| $C_1, C_2$ | = | constants used in turbulence model |
| $c_p$ | = | specific heat for constant pressure |
| $c_{p,\infty}$ | = | heat capacity of the gas |
| $D_p$ | = | droplet diameter |
| $E$ | = | empirical constant |
| $F_D$ | = | drag force per unit droplet mass |
| $F_i$ | = | additional forces such as body force, pressure force, and thermodynamic force |
| $G$ | = | generation rate of turbulent kinetic energy |
| $G_{ij}$ | = | primary generation or production rate of |
| $h$ | = | convective heat-transfer coefficient |
| $h_{\mathrm{fg}}$ | = | latent heat |
| $i$ | = | turbulence intensity |
| $k$ | = | turbulent kinetic energy |
| $k_1, k_2, k_3, k_4$ | = | thermal conductivity |
| $k_\infty$ | = | thermal conductivity of the gas |
| $L$ | = | pipe length |
| $Nu$ | = | Nusselt number |
| $P$ | = | $P$ function |
| $p$ | = | mean pressure |
| $Pr$ | = | Prandtl number |
| $Pr_t$ | = | turbulent Prandtl number |
| $\dot{q}$ | = | total heat flux |
| $\dot{q}''_w$ | = | wall heat flux per unit area |
| $r$ | = | radial coordinate |
| $S_\phi$ | = | source terms of transport equations in the discretization equation |
| $T$ | = | mean temperature |
| $T_f$ | = | fluid temperature |
| $T_{\mathrm{in}}$ | = | inlet stream velocity |
| $T_w$ | = | local wall temperature |
| $T_\infty$ | = | ambient temperature |
| $U$ | = | streamwise velocity component |
| $U_f$ | = | fluid velocity in a pipe |
| $U_{\mathrm{in}}$ | = | inlet velocity |
| $U_p$ | = | droplet particle motion velocity |
| $U_\tau$ | = | friction velocity |
| $U_\infty$ | = | velocities of the freestream steam flow |
| $u$ | = | turbulent fluctuating velocity |
| $\overline{u_i u_j}$ | = | Reynolds stresses |
| $V$ | = | mean velocity in $y$ direction |
| $W$ | = | mean velocity in $z$ direction |
| $X$ | = | steam quality |
| $x, y, z$ | = | Cartesian coordinates |
| $x_p$ | = | position of water particles |
| $y_f$ | = | normal distance from the wall to a point in the flow |
| $\Gamma$ | = | diffusion coefficient |

Received 4 March 1999; revision received 10 August 2001; accepted for publication 22 August 2001. 

*Professor, Department of Mechanical Engineering, EMS Building.
†Research Assistant, Department of Mechanical Engineering.
‡Research Assistant, Department of Mechanical Engineering.

$\delta_{ij}$ = Kronecker delta
$\varepsilon$ = dissipation rate of turbulent kinetic energy
$\varepsilon_{ij}$ = dissipation rate of $\overline{u_i u_j}$
$\theta$ = fluctuating temperature
$\kappa$ = von Kármán constant
$\Lambda$ = overall heat-transfer coefficient
$\mu$ = dynamic viscosity
$\nu$ = kinematic viscosity, $\mu/\rho$
$\nu_{\text{eff}}$ = effective kinematic viscosity, $\nu + \nu_t$
$\nu_t$ = kinematic eddy viscosity
$\xi, \eta, \zeta$ = curvilinear coordinates
$\rho$ = density of fluid
$\rho_p$ = particle droplet density
$\sigma$ = stress
$\tau$ = shear stress
$\phi_{ij}$ = pressure-strain correlations of $\overline{u_i u_j}$
$\bar{\phi}$ = time-averaged values of quantity $\phi$

*Subscripts*

av = averaged value
$f$ = values in fluid
$i, j$ = tensor notations
in = inlet station conditions
$v$ = values at viscous sublayer
$w$ = wall values

## Introduction

IN an industrial power plant combined-cycle system the performance of a cogenerator is equally as important as that of a main gas turbine power unit for an efficient operation. Mechanisms for controlling the steam temperature of a cogenerator in a bypass pipe system need to be carefully designed in order to enhance the system efficiency, to prevent failure of the components, and to increase unit life. To this end a high-pressure turbine bypass valve is always used to control the steam flow rate by abruptly reducing the steam pressure; the valve is followed by a steam cooling system for temperature reduction. In general, such steam temperature reduction of highly pressurized steam can be achieved by the inclusion of a cooling water injection spray system in a bypass pipe before the steam enters into a condenser. Thus, spray injection of cooling water into a superheated steam environment has been a subject of interest. Various studies seeking such an efficient cooling mechanism have been conducted during the past decade.[1] These have observed that the flows in the aforementioned flow-mixing process take place under a high-Reynolds-number turbulent flow. Thus, the turbulence effect significantly enhances the heat transfer, and, as a result, the evaporation process of water droplets is enhanced as well. Such enhancement is, mostly, based on geometrically created turbulence promoters such as perforated plates, orifices, elbows, diffusers, etc. Among these, a perforated plate has been occasionally adopted in many applications to enhance evaporation processes as well as to break larger droplets into smaller pieces and to disperse liquid droplets in a gaseous-phase flow. The inclusion of a perforated plate has some advantages over a pipeline: 1) it causes significant pressure reduction, and 2) it produces a higher mixture of steam and water droplets by reducing the droplet size by means of the collision of particles. This is similar to that result produced by devices designed on the basis of a turbulence eddy promoter. Although turbulent eddies arise from the instability of the flow, dispersion through a perforated plate is affected by the existence of the solid blockage and flow through narrow passages, which force the flow to undergo local transverse motion. This introduces an additional transport mechanism.

Many studies in conjunction with the problem just stated have been reported. Formulations of growth or attenuation of the liquid phase and thermal nonequilibrium properties were developed by Bakhtar and Mohammadi Tochai[2] and Young.[3] With regard to cooling technologies, cooling of high-temperature gas turbine flows in a rotating cavity was studied by Amano et al.[1] Findings for water spray jets mixing with ambient air were reported by Amano et al.,[4] where the turbulence modeling of water droplet dynamics was also addressed.

It was further observed in industries that flows in which liquid and gaseous phases mix are highly turbulent flows; thus, the turbulence effect is significant in effectively evaporating water droplets. For the simulations of steam flow behavior, both turbulence and numerical studies are crucial for a proper evaluation of the heat transfer and evaporation processes.

Numerous turbulence models using a higher-order closure model have been reported.[5–7] Another significant area of research related to the present problem is the impact of water droplets on a metal surface. This phenomenon is important not only in the present flow through a pipe with elbows but also in steam turbine blade flows. Experimental observations have been reported by Parker reported in Ref. 8, McAllister,[8] Traupel,[9] and others. Droplet breakup and deformation processes have been reported by Hassler[10] and Moore et al.[11]

The objective of the present study is to investigate the process that occurs when steam mixes with cooling water spray particles in a pipeline system downstream of a high-pressure turbine bypass valve and to observe the influence of property variations along the entire pipeline system up to the inlet of a condenser where the pressure suddenly drops down to a nearly vacuum condition. The effect of a perforated plate downstream of the cooling spray nozzles was also investigated.

To perform the studies just mentioned, computational methods were employed using a finite volume method. Modeling of the high-pressure turbulent steam flow was successfully accomplished using three-dimensional, turbulent, compressible, and two-phase dispersed flow formulations. The governing equations were discretized on a curvilinear grid to enable computations in irregular geometries. A nonstaggered grid system was used for discrete velocities and pressures. Interpolation was accomplished via the higher-order scheme. The investigation of the structure of a turbulent, liquid spray jet during the transition into the gaseous phase was performed by incorporating a physical model to investigate growth and dissipation processes of the liquid droplets in a highly turbulent flow. Turbulent flows were solved by incorporating a higher-order closure of turbulence in the model. Here the computations performed show very encouraging results when compared with experimental data and theoretical results.

## Physical Mathematical Models

Figure 1 shows a turbine bypass valve from which the pipeline is connected to a condenser. The steam at the exit of the valve is at about 7 atm of the pressures when in a full opening condition of the

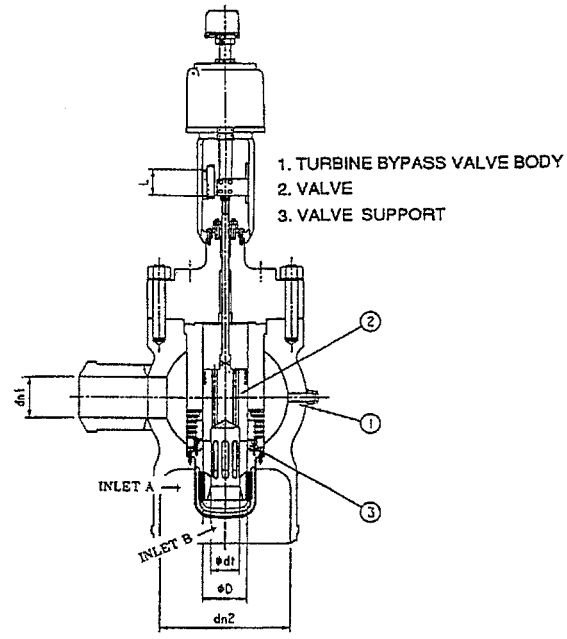


**Fig. 1 Schematic of the turbine bypass valve.**

valve. The steam is injected from the valve into the pipe through two labyrinth-type paths — one in the side of the valve (inlet A) and the other a drain hole with a 3.2-mm diameter at the center of the valve bottom (inlet B) — with the resulting steam flow at 7 atm after passing through a bypass valve.

The overall pipe system (0.645 m in diameter) is approximately 20 pipe diameters (13 m) long. A schematic of the pipe system is shown in Fig. 2, where there are four 90 degree elbows along the pipeline. The entire system was divided into four sections as shown in the figure; i.e., pipe I–IV. Pipe I is the straight section where the top portion is the bypass valve exit.

Two sets of cooling water spray nozzles are mounted; three spray nozzles (nozzle A) are mounted at 0.75 m and three spray nozzles (nozzle B) at 1.0 m, respectively, downstream from the exit of the valve. Each set contains three nozzles spaced 120 degree apart. In addition to the different vertical locations of the jets, the upper (nozzle A) and lower (nozzle B) jets are spaced 60 degree apart. A total mass flow rate of 1.66 kg/s is injected through nozzle A and a total of 15.84 kg/s through nozzle B.

The just-mentioned conditions used in this study are a typical steam flow for such valves with a full open. These are listed in Table 1.

Pipe II starts slightly upstream of the first elbow and ends at the section slightly upstream of the second elbow so that the flow from pipe I has almost reached a fully developed consition. Similarly, pipe III starts at the exit of pipe II and ends at the section slightly upstream of the third elbow. Pipe IV consists of the rest of the pipeline including the fourth elbow to the end where the pipe is connected to the condenser.

**Table 1 Inlet conditions**

| | Inlet A | Inlet B | Nozzle A | Nozzle B |
|---|---|---|---|---|
| Fluid | Steam | Steam | Water droplet | Water droplet |
| Mass flow rate, kg/s | 78.91 | 0.115 | 1.66 | 15.84 |
| Velocity, m/s | 192.6 | 185.9 | 65.0 | 65.0 |
| Temperature, K | 756 | 756 | 303 | 303 |
| Pressure, atm | 7 | 7 | —— | —— |
| Density, kg/m$^3$ | 1.972 | 72 | 998.2 | 998.2 |
| Boiling point, K | —— | —— | 438 | 438 |
| Specific heat, kJ/kg K | 2.940 | 2.940 | 4.178 | 4.178 |
| Viscosity, kg m/s $10^5$ | 60 | 2.560 | 100.4 | 100.4 |
| Thermal conductivity, W/m K | 0.690 | 0.690 | 0.620 | 0.620 |
| Latent heat, J/kg $10^{-6}$ | 2.4239 | 2.4329 | 2.4329 | 2.4329 |
| Droplet size, $\mu$m | —— | —— | 350 | 750 |

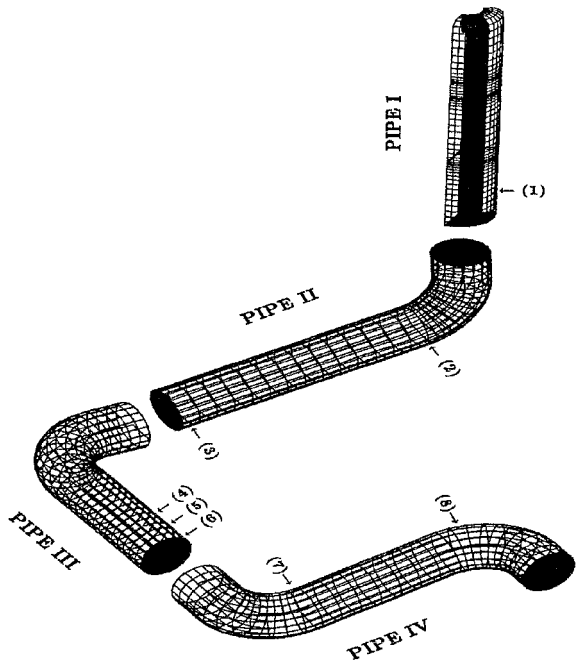


**Fig. 2 Schematic of the pipeline system.**

At the end of pipe IV, the steam is directed into a condenser through a diffuser by dropping the pressure down to 4,900 Pa. Thus, a diffuser model is installed here at the end of pipe IV.

Another consideration in the flow study concerns the effects of a perforated plate, which is mounted at a location 0.8 m downstream from nozzle B. The purpose of insertion of a perforated plate is to force larger size of water droplets break into smaller particles so that it accelerates the surviving droplets to evaporate.

### Governing Equations

Flows through a pipe can be governed by differential equations consisting of continuity, momentum, and energy equations. The main steam flow calculations consist of the compressible three-dimensional Navier–Stokes equations combined with the energy and the full Reynolds-stress equations. The mixture conservation equations were solved in an Eulerian reference frame. The equation of state of the vapor phase was solved for the density, enthalpy, entropy, and quality. Nonequilibrium thermodynamic properties were computed for the steam properties.

The basic conservation equations, expressed in vector form using the summation convention for repeated indices, are written as follows:

Continuity:

$$\partial_t \rho v + \partial_i \rho \boldsymbol{W} \cdot \boldsymbol{S} = 0 \tag{1}$$

Momentum:

$$\partial_t \rho \boldsymbol{U} v + \partial_i (\rho \boldsymbol{U}\boldsymbol{W} + \sigma) \cdot \boldsymbol{S}_i = \boldsymbol{H}_u \tag{2}$$

Energy:

$$\partial_t \rho E v + \partial_i (\rho E \boldsymbol{W} + \boldsymbol{U} \cdot \sigma + \boldsymbol{q}_\kappa) \cdot \boldsymbol{S}_i = \boldsymbol{H}_E \tag{3}$$

Turbulence kinetic energy:

$$\partial_t \rho k v + \partial_i (\rho k \boldsymbol{W} + \boldsymbol{q}_\kappa) \cdot \boldsymbol{S}_i = \boldsymbol{H}_\kappa \tag{4}$$

Turbulence energy dissipation:

$$\partial_t \rho \varepsilon v + \partial_i (\rho \varepsilon \boldsymbol{W} + \boldsymbol{q}\varepsilon) \cdot \boldsymbol{S}_i = \boldsymbol{H}_\varepsilon \tag{5}$$

Reynolds stresses:

$$\partial_t \rho \overline{u_i u_j} v + \partial_i (\rho \overline{u_i u_j} \boldsymbol{W} + \boldsymbol{q}_{ij}) \cdot \boldsymbol{S}_i = \boldsymbol{H}_{ij} \tag{6}$$

where

$$\partial_i = \frac{\partial}{\partial \xi_i} \tag{7}$$

and where $\xi$ represents curvilinear coordinate variables.

### Stochastic Particle Tracking

A stochastic particle tracking method was employed for tracing the water droplets in steam turbulent flows. This method incorporates the instantaneous values of the fluctuating components in the gas flow velocities. The trajectory of a water droplet is predicted on a Lagrangian reference frame. The force of a droplet per unit mass is given by

$$\frac{\mathrm{d}U_p}{\mathrm{d}t} = F_D(U_\infty - U_p) + \frac{g(\rho_p - \rho_\infty)}{\rho_p} + F_i \tag{8}$$

The drag force was estimated by using the drag coefficient $C_D$ determined from Oseen's approximation for a particle Reynolds number less than 1000 and 0.424 for a Reynolds number larger than 1000.

The additional force $F_i$ consisting of the force caused by particle acceleration and the pressure forces are given by

$$F_{\mathrm{accl}} = \frac{1}{2}\frac{\rho_\infty}{\rho_p}\frac{\mathrm{d}}{\mathrm{d}t}(U_\infty - U_p) \tag{9}$$

and

$$F_{\text{press}} = \frac{\rho_\infty}{\rho_p} U_\infty \frac{\partial U_\infty}{\partial x} \tag{10}$$

The particle path is determined by using the stochastic particle tracking method in which the instantaneous values of the fluctuating components in the turbulent steam flow velocities is

$$U_i = \boldsymbol{U}_i + u_i \tag{11}$$

The values of the turbulence fluctuation $u_i$, which prevails during the lifetime of a fluid eddy that fluid particle is traveling, are sampled by assuming that they obey a Gaussian probability distribution, so that

$$u_i = \lambda \sqrt{\overline{u_i^2}} \tag{12}$$

where $\lambda$ is a normal distributed random number. The Reynolds stresses appearing in the square root in Eq. (12) are evaluated through the Reynolds-stress model.[6,7,12]

The complete range of particle sizes is divided into an adequate number of discrete intervals, each represented by a mean diameter for which trajectory calculations are performed.

The position of a liquid particle can be evaluated by

$$\frac{\mathrm{d}x_p}{\mathrm{d}t} = U_p \tag{13}$$

During the integration, the fluid phase velocity $U$ can be taken as the cell-based velocity for all particle positions within the cell, or it can be taken as the velocity at the particle position.

**Evaporation Model**

Nucleation or evaporation of water droplets was evaluated along streamlines using a Lagrangian reference frame. The results are stored as parameters for the full viscous momentum equations. The growth or attenuation of the liquid phase and thermal nonequilibrium properties were obtained following Bakhtar and Mohammadi Tochai[2] and Young.[3]

The boiling mechanism is such that the droplet is assumed to stay at a constant temperature while the boiling rate is applied. Once the boiling law is employed, it is applied for the duration of the particle trajectory. The energy required for vaporization is treated as a sink term in the energy equation for the gas phase.

In summary, the onset of the vaporization is determined by setting the vaporization temperature at the associated pressure level. When the temperature of a droplet reaches its boiling point, the droplet vaporization is predicted by a boiling rate

$$\frac{\mathrm{d}D_p}{\mathrm{d}t} = -\frac{C_b}{2D_p}\left(1 + 0.23Re^{\frac{1}{2}}\right) \tag{14}$$

where the coefficient is given by Williams[13]:

$$C_b = \frac{8\kappa_\infty}{\rho_p c_{p,\infty}} \ell n\left[1 + \frac{c_{p,\infty}}{h_{\text{fg}}}(T_\infty - T_p)\right] \tag{15}$$

**Heat Transfer**

The heat-transfer mechanism is one of the most important items that needs to be studied in a greater detail because the evaporation rate of the water droplet is significantly affected by the steam temperature. To this end the heat transfer through the pipe wall and the insulation materials should be evaluated accurately as well as the heat transfer between water droplets and the steam. The steam temperature varies significantly depending on the wall condition. For example, if the wall is assumed to be adiabatic the steam exchanges heat only with water droplets. However, if the pipe is insulated but still allows heat loss to the ambient air outside the pipeline the steam temperature drops accordingly. For this reason a study of three modes of the heat transfer was conducted: 1) convective heat transfer between water droplets and steam, 2) convective heat-transfer rate between the fluid and the pipe wall, and 3) conjugate heat transfer through the composite material consisting of pipe wall and insulation materials.

*Convective Heat Transfer Near the Wall*

The heat-transfer coefficient was determined by using an analogy between momentum and the heat-transfer mechanism, which is applicable in the near-wall region. This empirical wall function accounts for viscous sublayer effects via the turbulence kinetic energy at the edge of the viscous sublayer. From the law of the wall, we have

$$\frac{U_f k_v^{\frac{1}{2}}}{\tau_w/\rho} = \frac{1}{\kappa} \ell n\left(E \frac{y_f k_v^{\frac{1}{2}}}{\nu}\right) \tag{16}$$

where $U_f$ denotes the mean fluid velocity at a position in the flowfield in the boundary layer and $y_f$ the corresponding distance from the wall. The empirical constants $E$ and $\kappa$ are related to the original von Kármán constants and have values of 5.0 and 0.23, respectively. The wall shear stress $\tau_w$ is evaluated through the extrapolation of the turbulent shear stresses to the wall. The turbulence kinetic energy $k_v$ represents the value at the viscous sublayer, which was computed with the parabolic variation in the viscous sublayer and the extrapolation from the turbulence kinetic energy values at outer regions.[14] Upon using the preceding description, Eq. (16) for the heat-transfer rate can be given as

$$\frac{\rho c_p (T - T_w)(\overline{u_i u_j}/2)^{\frac{1}{2}}}{\dot{q}_w''} = \frac{U(\overline{u_i u_j}/2)^{\frac{1}{2}}}{\tau_w/\rho} + P \tag{17}$$

Moreover, the preceding expression is equivalent to the following under the local isotropic condition:

$$\frac{(T_f - T_w)\rho c_p k_v^{\frac{1}{2}}}{\dot{q}_w''} = \frac{1}{\kappa} \ell n\left(E \frac{y_f k_v^{\frac{1}{2}}}{\upsilon}\right) + P \tag{18}$$

where $P$ is the so-called $P$ function, which was proposed by Jayatilleke[15] and is given by

$$P = 9.24\left[\left(\frac{Pr}{Pr_t}\right)^{0.75} - 1\right]\left[1 + 0.28\exp\left(-0.007\frac{Pr}{Pr_t}\right)\right] \tag{19}$$

The turbulent Prandtl number was set equal to 0.9.

Once the heat-transfer coefficient was known, the local heat flux, as well as the local wall temperature profile, was obtained. The wall was modeled as two 30-mm layers of insulation followed by a thin covering material that sat on top of a thin layer of air.

Local heat-transfer coefficients are computed from

$$h = \dot{q}_w''/(T - T_w) \tag{20}$$

where the wall flux rate can be determined by employing the "wall law." This is further given by

$$h_i = \frac{\rho c_p k_v^{\frac{1}{2}}}{Pr_t\left[(1/\kappa)\,\ell n\left(E y_p k_v^{\frac{1}{2}}/\upsilon\right) + P\right]} \tag{21}$$

The turbulent Prandtl number $Pr_t$ is set equal to 0.9.

*Conjugate Heat Transfer*

The cross section of the pipe system is illustrated in Fig. 3. Through the pipe wall and the insulation materials the heat-conduction rate is determined by

$$\dot{q} = \Lambda A_5 (T_f - T_\infty) \tag{22}$$

where $\Lambda$ is given by

$$\Lambda = \left( \frac{A_5}{A_1}\frac{1}{h_i} + \frac{A_5}{2\pi k_1 L A_1}\ell n\frac{r_2}{r_1} + \frac{A_5}{2\pi k_2 L A_2}\ell n\frac{r_3}{r_2} + \frac{A_5}{2\pi k_3 L A_3}\ell n\frac{r_4}{r_3} + \frac{A_5}{2\pi k_4 L A_4}\ell n\frac{r_5}{r_4} + \frac{1}{h_o}\right)^{-1} \tag{23}$$

Here A's represents the surface areas of the solid wall and is given as

$$A_i = 2\pi r_i L \qquad i = 1 \sim 5$$

and the thermal conductivities of the materials are

$$k_1 = 0.0414 \exp[0.0024 T_{\text{av}}] \text{ W/mK}$$

$$k_2 = 0.0414 \exp[0.0024 T_{\text{av}}] \text{ W/mK}, \qquad k_3 = k_{\text{air}} = 0.45 \text{ W/mK}$$

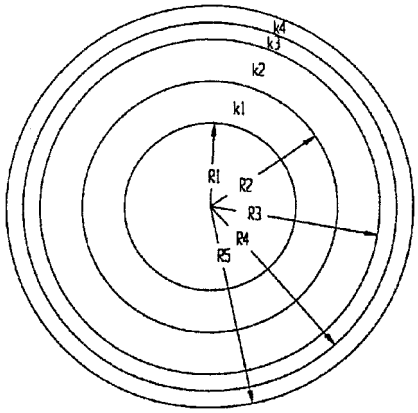


**Fig. 3 Heat conduction through the pipe wall and insulators.**

$$k_4 = 0.0507 \exp[0.002 T_{\text{av}}] \text{ W/mK}$$

Therefore, the wall temperatures are determined as

$$T_{w1} = T_f - \frac{\dot{q}}{A_1 h_f} \tag{24}$$

$$T_{w2} = T_{w1} - \dot{q}\frac{\ell n(r_2/r_1)}{2\pi k_1 L} \tag{25}$$

$$T_{w3} = T_{w2} - \dot{q}\frac{\ell n(r_3/r_2)}{2\pi k_2 L} \tag{26}$$

$$T_{w4} = T_{w3} - \dot{q}\frac{\ell n(r_4/r_3)}{2\pi k_3 L} \tag{27}$$

$$T_{w5} = T_{w4} - \dot{q}\frac{\ell n(r_5/r_4)}{2\pi k_4 L} \tag{28}$$

*Water Droplets*

The heat-transfer rate between a water droplet and the environmental steam can be evaluated by using the following relation:

$$Nu = 2 + 0.60\, Re^{\frac{1}{2}} Pr^{\frac{1}{3}} \tag{29}$$

**Numerical Method**

The transport equations used in the study were transformed into a three-dimensional curvilinear coordinate system.

The flow pass configuration was created by employing a grid-generation technique based on the two-dimensional internal flow grid generation.[16,17] This method is particularly advantageous for computations of a flow that is bounded by solid boundaries. Actually, it was shown that employing a generation step is much simpler than using the body-fitted adaptive grid-generation method.

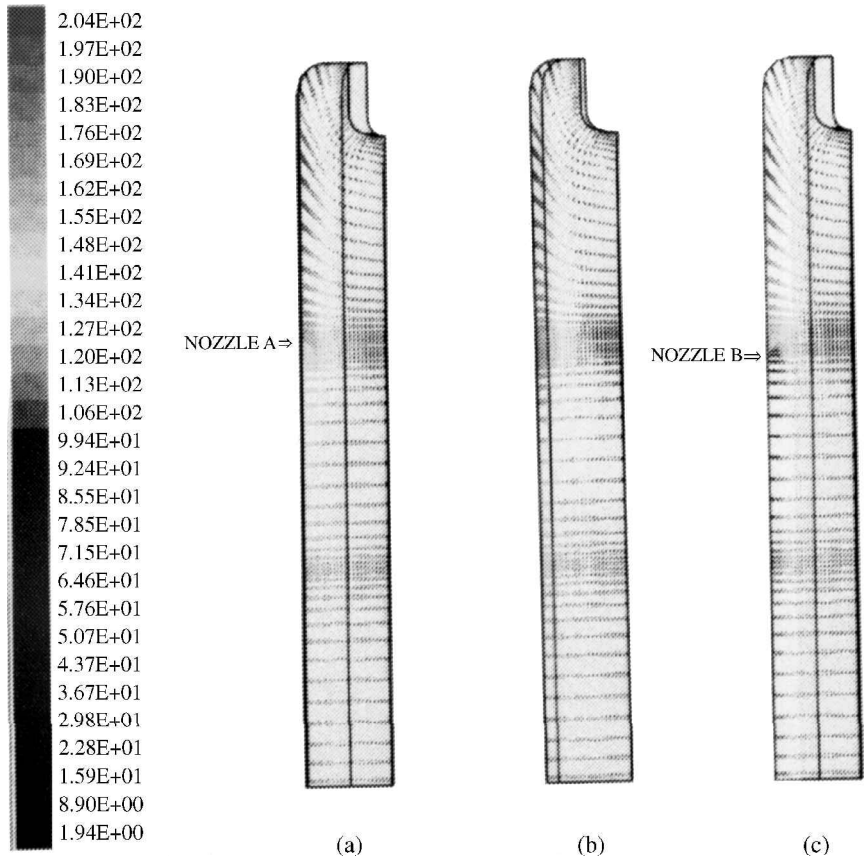


**Fig. 4 Velocity vectors along longitudinal slices in Pipe I: a) Plane that contains nozzle A, b) Midplane between planes a) and b), and c) Plane that contains nozzle B.**

For general three-dimensional configurations it is usually very difficult to obtain a reasonable grid with the entire physical region transformed into a single rectangular block. The technique used in this study follows the path of Thompson.[16] In this approach complete continuity can be achieved at the subregion interfaces by noting the correspondence of points exterior to one subregion with points interior to another. The necessary bookkeeping can be accomplished, and the coding complexity can be greatly reduced by using an auxiliary layer of points just outside each of the six sides of the computational region, analogous to the procedure for two dimensions. A correspondence is then established in the code between the auxiliary points and the appropriate points just inside other subregions.

General three-dimensional regions can be built up using subregions. First, point distributions are specified on the edges of a curved surface forming one boundary of a subregion, and a two-dimensional coordinate system is generated on the surface. When this has been done for all surfaces bounding the subregion, the three-dimensional system within the subregion is generated using the points on the surface grids as boundary conditions. All of these steps can be performed interactively so that the user is able to monitor the generation and alter the grid by varying parameters.

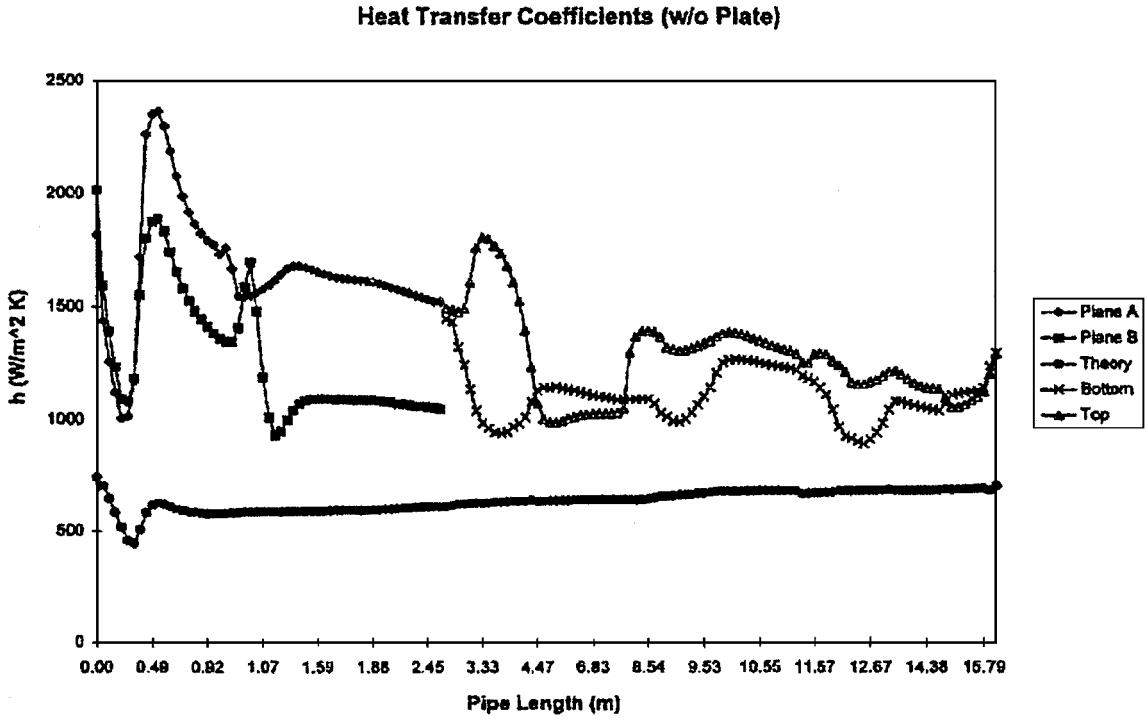


**Local heat-transfer coefficient**

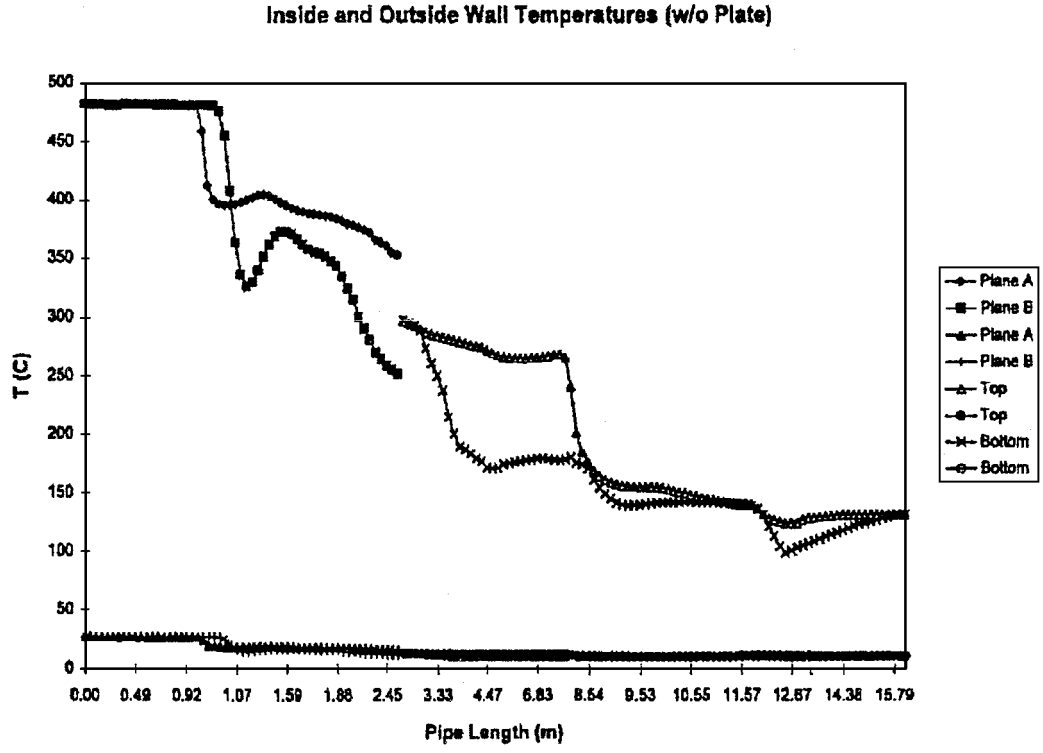


**Temperature along the wall and insulators**

**Fig. 5 Wall heat transfer through the pipeline.**

$$\frac{\partial \rho\phi}{\partial t} + \frac{\partial(\rho U\phi)}{\partial x} + \frac{\partial(\rho V\phi)}{\partial y} + \frac{\partial(\rho W\phi)}{\partial z} = \frac{\partial}{\partial x}\left(\Gamma\frac{\partial\phi}{\partial x}\right) + \frac{\partial}{\partial y}\left(\Gamma\frac{\partial\phi}{\partial y}\right) + \frac{\partial}{\partial z}\left(\Gamma\frac{\partial\phi}{\partial z}\right) + R(x, y, z) \tag{30}$$

where

$$\phi = U : R(x, y, z) = \frac{\partial p}{\partial x} + S_u \tag{31}$$

$$\phi = V : R(x, y, z) = \frac{\partial p}{\partial y} + S_v \tag{32}$$

$$\phi = W : R(x, y, z) = \frac{\partial p}{\partial z} + S_w \tag{33}$$

$$\phi = k : R(x, y, z) = \rho(G - \varepsilon) + S_k \tag{34}$$

$$\phi = \overline{u_i u_j} : R(x, y, z) = \rho(G_{ij} - \varepsilon_{ij}) + \Phi_{ij} + S_{ij} \tag{35}$$

$$\phi = \varepsilon : R(x, y, z) = \rho\frac{\varepsilon}{k}(C_1 G - C_2\varepsilon) + S_\varepsilon \tag{36}$$

where $G$ and $G_{ij}$ denote the turbulence energy generation rates for $k$ and $\overline{u_i u_j}$, respectively. Similarly, $\varepsilon$ and $\varepsilon_{ij}$ represent the turbulence energy dissipation rates for $k$ and $\overline{u_i u_j}$, respectively.

The preceding equation is transformed into the following form:

$$\frac{1}{J}\frac{\partial\rho\phi}{\partial t} + \frac{1}{J}\left[\frac{\partial(\rho\tilde{U}\phi)}{\partial\xi} + \frac{\partial(\rho\tilde{V}\phi)}{\partial\eta} + \frac{\partial(\rho\tilde{W}\phi)}{\partial\zeta}\right] = \frac{1}{J}\left[\frac{\partial}{\partial\xi}\left(\frac{\Gamma}{J}Q_\xi\right) + \frac{\partial}{\partial\eta}\left(\frac{\Gamma}{J}Q_\eta\right) + \frac{\partial}{\partial\zeta}\left(\frac{\Gamma}{J}Q_\zeta\right) + S(\xi, \eta, \zeta)\right] \tag{37}$$

where $J$ denotes Jacobian, and where $\tilde{U}$, $\tilde{V}$, and $\tilde{W}$ represent contravariant velocities in $\xi$, $\eta$, and $\zeta$ coordinates, respectively. $Q_\xi$, $Q_\eta$, and $Q_\zeta$ show the flux rate for $\xi$, $\eta$, and $\zeta$ coordinate variables, respectively.

The equations are solved using the SIMPLEC algorithm with an iterative line-by-line matrix solver and a multigrid acceleration solver by VanDoormaal and Raithby,[18] Hutchinson et al.,[19] and Peric.[20]

Extensive grid-independent tests have been performed with the grid systems varying from 30,000 to 100,000 and found that the grid-independent state has been achieved with the grids more than 50,000. Therefore, a grid of $42 \times 25 \times 62$ is used for pipe I, which is one-sixth of the complete pipeline in the radial, azimuth, and axial directions, respectively. For the other pipes a grid of $39 \times 21 \times 31$ is used in the radial, azimuth, and axial directions, respectively. These grids are arranged to have a much denser distribution in the near-wall region while they are relatively scarcely arranged in the region toward the center of the pipe. Therefore, the results are grid independent in comparison with different numbers of the grid.

## Presentation of Results

Two sets of computational results are presented in this section: one without a perforated plate inserted and the other with the plate inserted.

### Velocity

Cutaway views of velocity vectors are illustrated in Fig. 4 for pipe I flows. In Fig. 4 the first longitudinal slice shows the velocity map on the plane, which contains nozzle A. The third longitudinal slice shows the velocity map on the plane, which contains nozzle B. These two planes are at a 60-deg angle apart from each other. The second slice in these figures lies between the first and the third planes, which were just described, at a 30E angle from each other. As shown in these figures, the highest velocity occurs along the wall opposite to and just below the main stream inlet (inlet A). This velocity increase occurs after the initial impingement of the steam flow on the pipe wall by accelerating to the maximum from the impingement point (shown in red). The average velocity of the steam through the whisper gage (labyrinth) at the exit of the bypass valve (inlet A) is about 186 m/s caused by the steam mass flow rate of 78.91 kg/s.

Of note in these figures is the abrupt change in velocity when the flow encounters the water spray injection nozzles. This is most clearly viewed in Fig. 4c, where each nozzle B is injecting 5.2 kg/s of water into the steam flow (there are three injection nozzles with a total flow rate of 15.8 kg/s). At this location the velocity drops from 140 to 70 m/s. A velocity reduction also occurs at nozzle A. However, the mass flow of nozzle A is only one-tenth that of nozzle B, and thus the velocity drop is significantly smaller. These figures also show that the flow has not fully developed before it leaves the

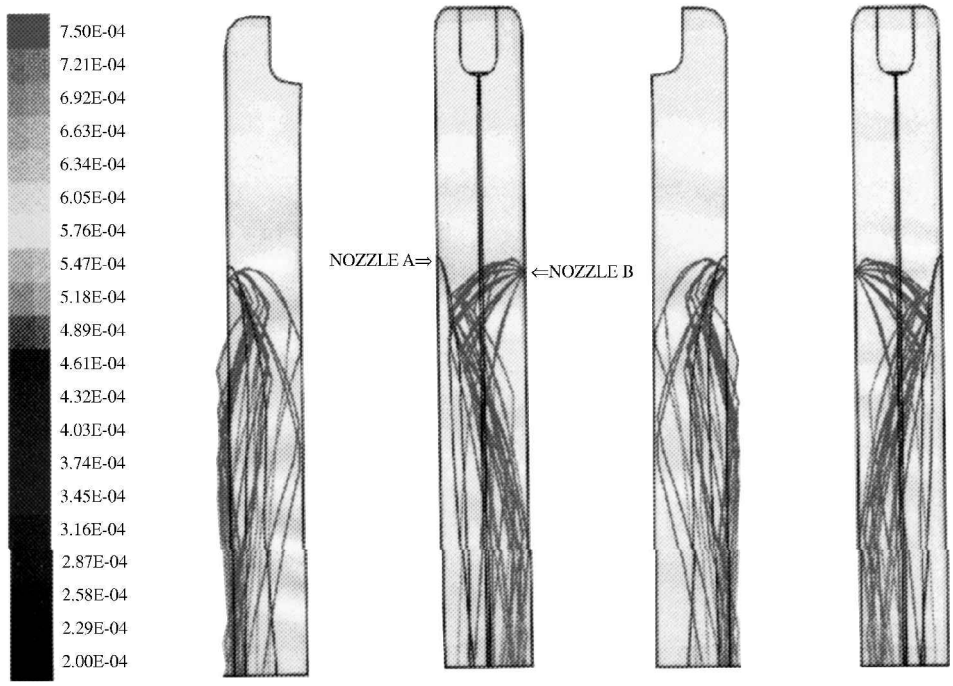


**Fig. 6 Particle tracking view at different angle of the pipe in pipe I.**

section. In Figs. 4a and 4b the velocity is still greater along the wall than at the center of the pipe.

Although there is another steam injection through a drain hole at the centerline of the pipe (inlet B), the flow rate there is small (0.115 kg/s), and therefore it does not appear clearly in the figure.

### Heat Transfer

The variations of the computed heat-transfer coefficients along the inner wall of the pipe are shown in Fig. 5 along two different longitudinal lines; one along the plane containing nozzle A, and the other along the plane that contains nozzle B. Significant effects of the steam impingement and the spray are clearly observed in these curves.

The injection of the cooling water apparently enhances the heat-transfer coefficient. These results are also compared with the fully developed turbulent flow heat-transfer coefficient given by Dittus and Boelter[21]:

$$Nu_D = 0.023\, Re_D^{0.8} Pr^{0.3} \tag{38}$$

The computed heat transfer behaves in a rather complex manner. It sharply drops at the starting location where the steam just expands at the valve exit followed by a rapid increase as a result of the flow impingement on the pipe wall. It seems the computed heat-transfer coefficients approach the Dittus–Boelter curve as one goes downstream of the flow. The heat-transfer coefficient monotonically increases toward the exit of the pipe.

This is mainly because the Prandtl number decreases as temperature increases in the range of the current conditions. Therefore, while the steam keeps losing its temperature by exchanging heat between water droplets and rejecting heat to the pipe wall, the level of Prandtl number increases along the pipeline.

The wall-temperature distributions computed by using the heat-transfer coefficients just mentioned are also shown in Fig. 5. The wall temperature on the outermost wall of the insulator is about 25°C, which agrees very well with the experimentally measured temperature by Toshiba Corporation at Yokohama Power Plant site (Chiba, J., and Takahashi, A., Private communications, 1996). The experimental data for temperature were obtained by the researchers at Toshiba Corporation, and the results are compared with the present computations (Table 1). As shown here, the maximum error did not exceed 7%.

### Water Droplets

The injections from nozzles A and B are shown in Fig. 6, and those in the downstream sections through elbows are in Fig. 7. The distributions of the particles are also illustrated by a particle diameter. It is evident from these figures that the diameters change very

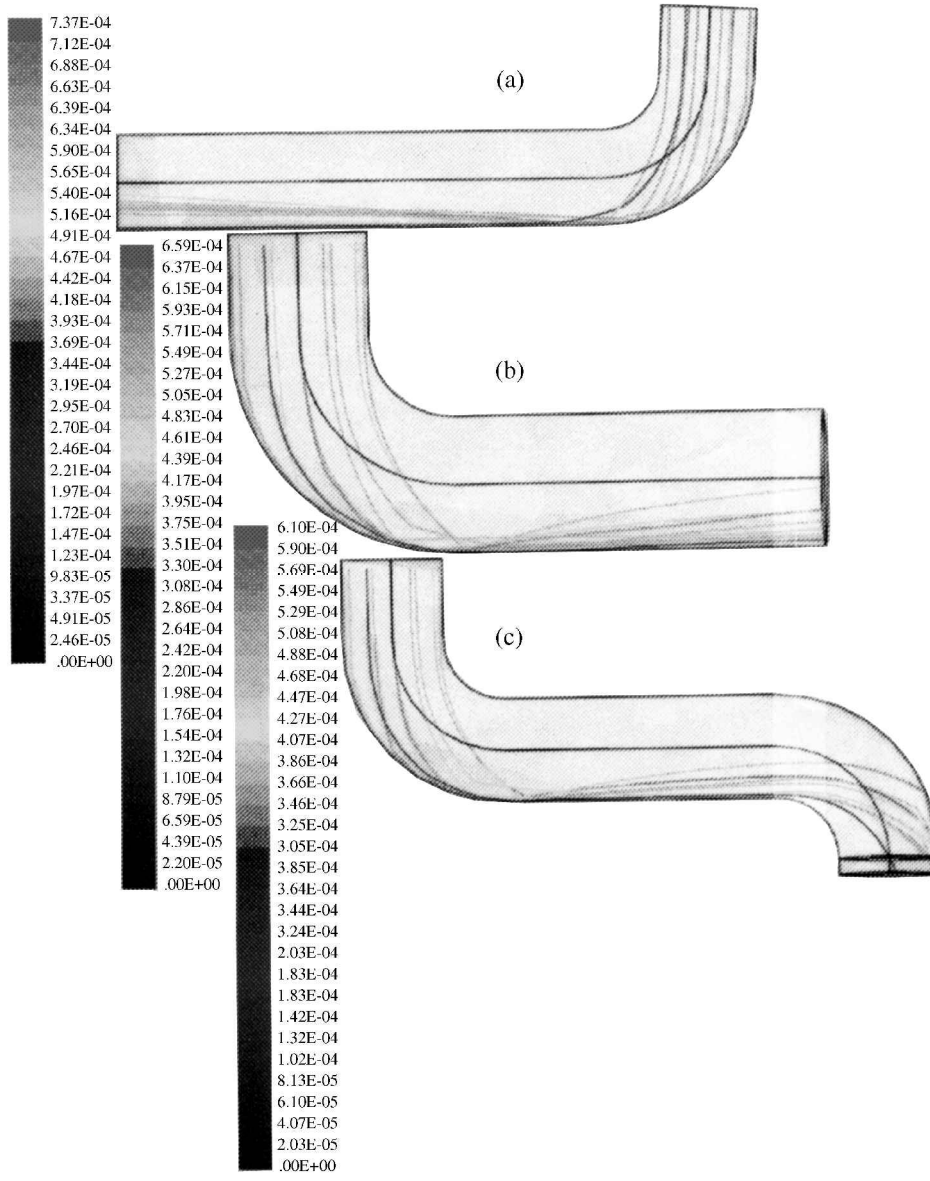


**Fig. 7 Particle tracking view at different angle of the pipe in pipes II–IV.**

little as they pass through the pipe. Though not shown, it was found that the particles quickly reached their saturation boiling points of 438 K (165°C) just after being injected into the steam flow. However they lose very little mass. The particle tracks do appear to distribute themselves throughout the section, giving a relatively even cooling effect. The apparent reflection of the tracks off of the walls is caused by the symmetry boundary condition imposed on the edges of the test section.

Along the elbows all of the particles impinge on the outer side of the wall and restore the momentum about 50% downward. This effect causes the concentration of the particles along the outer half of the pipe section by cooling the steam more in these regions. Another effect of the impingement of the particles onto the cooling of the wall is the resulting drop of the temperature on the pipe wall.

The distributions of particle sizes are shown in Fig. 8 as a function of particle diameter. As is apparent in the figure, particles are broken up into smaller sizes as they flow down. However, it is noteworthy that particles that are already small do not change size easily.

Finally, the percentage of mass flow rate of the water droplets is shown in Fig. 9. Two computations are compared in this figure; one with the original layout and the other when a perforated plate is inserted in the pipe path about one pipe diameter downstream from the water spray injection nozzles. The results in this figure indicate that effect of the perforated plate is significant in the upstream parts

**Table 2 Temperature (K) on the inner wall of the pipe**

| Position, $z/D$ | Experiment | Computation | Error, % |
|---|---|---|---|
| 17.3 | 498 | 501 | 6.02 |
| 17.6 | 412 | 20 | 1.94 |
| 17.8 | 452 | 449 | 0.70 |

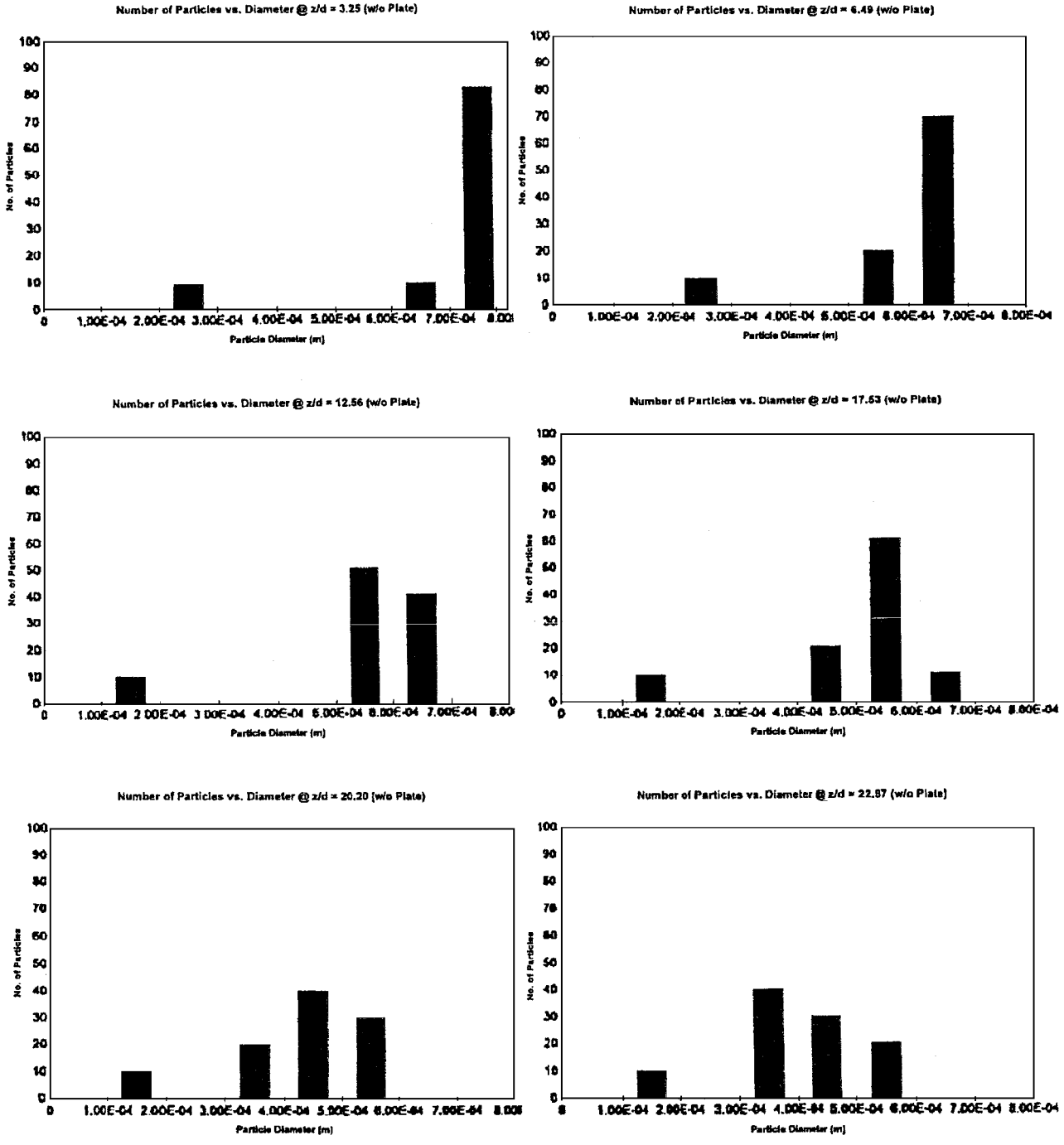


**Fig. 8 Particle distribution as a function of particle diameter.**

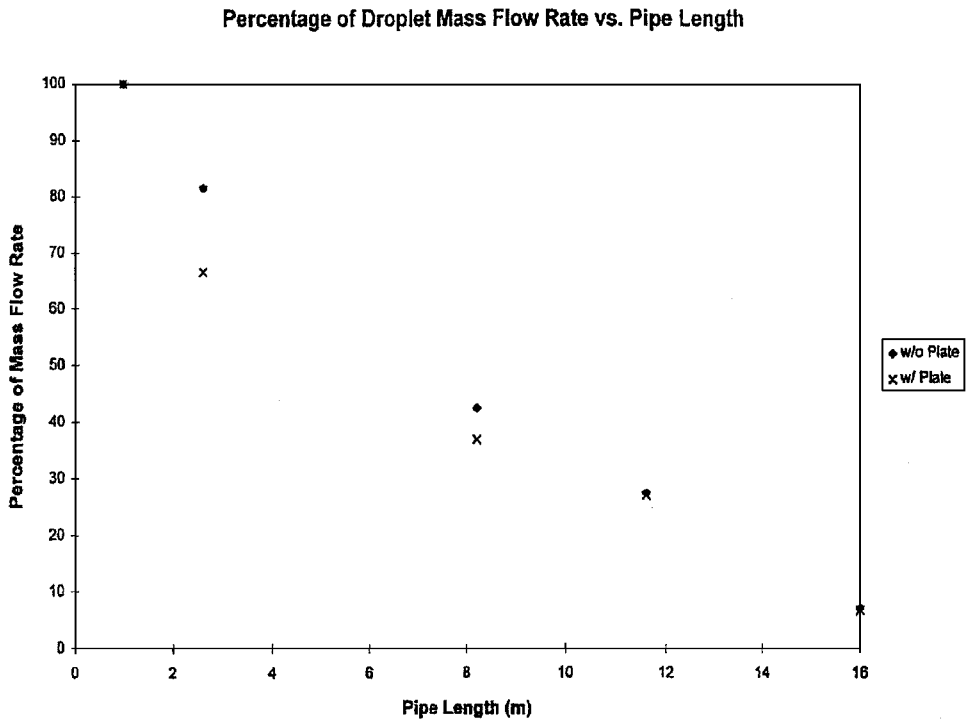


**Fig. 9 Particle distribution as a function of particle diameter.**

of the pipe. However, its effect diminishes toward the exit of the pipe.

## Conclusions

Through this study, first, the formulations using two-phase dispersed turbulence modeling were demonstrated to be successful in predicting steam flowfields laden with water droplets. Second, the trajectory and the Eulerian physical processes were demonstrated. Third, computations of turbulence stresses were accomplished, and the heat-transport process was correlated with the turbulence distributions throughout the flow passage. Finally, the evaporation process of the liquid droplets through a pipeline system was correlated with turbulence shearing action along a pipe path. Altogether this study clearly illuminated the process of mixing high-temperature steam with a cooling water spray in a complex, turbulent flow. Several significant conclusions emerged from this study are summarized as follows:

1) Significant heat transfer occurs through the pipe wall, which considerably reduces the steam temperature near the wall and results in a reduction in the evaporation rates of the water droplets in comparison with the case when the computations were performed by assuming the wall is adiabatic.

2) It was observed that the effect of the elbows on the water droplet path is to shift the droplets toward the outer side of the pipe. In other words, the particles are forced to flow toward the outer direction along the elbow. Therefore, the droplets hitting on the outer wall cause cooling of the fluid near the wall along the outer curvature surface of the pipe.

3) The effect of the perforated plate on the evaporation rate is to increase it by approximately 20% more than the case without a perforated plate. However, the survival amount of the water droplets at the end of the pipeline is about 10% of the injected water droplets, regardless of the insertion of the plate.

4) In the present case, if the data of McAllister[8] apply, almost all of the smaller droplets would adhere on the water films, whereas larger droplets break into fractions every time they hit on the wall at the elbows. Therefore, it is anticipated that at the end of the pipeline no particles exist at all.

## Acknowledgments

Most of the computations were made on a supercomputer (Power Challenge Array) which is supported by National Science Foundation (NSF) under Grant NSF CTS 950012N, 960022N, and 970045N. The research is supported by Moritani and Co. The authors are grateful for numerous suggestions made by the staff at Toshiba Corporation and Nippon Fisher Company Ltd.

## References

[1] Amano, R. S., Wang, K. D., and Pavelic, V., "A Study of Rotor Cavities and Heat Transfer in a Cooling Process in a Gas Turbine," *Journal of Turbomachinery*, Vol. 116, No. 2, 1994, pp. 333–338.

[2] Bakhtar, F., and Mohammadi Tochai, M. T., "An Investigation of Two-Dimensional Flows of Nucleating and Wet Steam by the Time-Marching Method," *International Journal of Heat and Fluid Flow*, Vol. 2, No. 1, 1980, pp. 5–18.

[3] Young, J. B., "Semi-Analytical Techniques for Investigating Thermal Non-Equilibrium Effects in Wet Steam Turbines," *International Journal of Heat and Fluid Flow*, Vol. 5, No. 21, 1984, pp. 81–91.

[4] Amano, R. S., Neusen, K. F., and Gores, T., "A Study of High-Speed Water Jet-Cutting Mixing Chamber," *Journal of Materials Processing and Manufacturing Science*, Vol. 1, No. 4, 1993, pp. 355–368.

[5] Launder, B. E., Reece, G. J., and Rodi, W., "Progress in the Development of a Reynolds-Stress Turbulence Closure," *Journal of Fluid Mechanics*, Vol. 68, Pt. 3, 1975, pp. 537–566.

[6] Amano, R. S., Goel, P., and Chai, J. C., "Turbulence Energy and Diffusion Transport of Third-Moments in a Separating and Re-Attaching Flow," *AIAA Journal*, Vol. 26, No. 3, 1988, pp. 273–282.

[7] Chai, J. C., and Amano, R. S., "Application of Higher-Order Turbulence Closure Model to Plane Jet," *Numerical Heat Transfer*, Vol. 21, Pt. A, 1992, pp. 21–35.

[8] McAllister, D. H., "The Collision of Drops with Dry and Wet Surfaces in an Air Atmosphere," *Proceedings on Institute of Mechanical Engineering, London*, Vol. 184, Pt. 3G, 1969–1970, pp. 78, 79.

[9] Traupel, W., *Thermische Turbomachinen*, Auflage Band 1, Vol. 1, Springer-Verlag, Berlin, 1962.

[10] Hässler, G., "Untersuchungen zur Verformung und Aufösung von Wassertropfen," Ph.D. Dissertation, Univ. of Karlsruhe, Germany, 1971.

[11] Moore, M. J., Langford, R. W., and Tipping, J. C., "Wet Steam," *Research at C.E.R.L. on Turbine Blade Erosion, Institute of Mechanical Engineering Conference*, Bristol, 1968, pp. 1–8.

[12] Amano, R. S., and Chai, J. C., "Transport Models of the Turbulent Velocity-Temperature Product for Computations of Recirculating Flows," *Numerical Heat Transfer*, Vol. 14, No. 1, 1988, pp. 75–95.

[13] Williams, F. A., *Combustion Theory*, Benjamin-Cummings Publishing Co., 1985.

[14] Amano, R. S., "Development of Turbulent Near-Wall Model and Its Application to Separated and Reattached Flow," *Numerical Heat Transfer*, Vol. 7, No. 1, 1984, pp. 59–70.

[15]Jayatilleke, C. L., "The Influence of Prandtl Number and Surface Roughness on the Resistance of the Laminar Sub-Layer to Momentum and Heat Transfer," *Progress in Heat and Mass Transfer*, Vol. 1, 1969, pp. 193–329.

[16]Thompson, J. F., "Numerical Solution of Flow Problems Using Body-Fitted Coordinate Systems," *Computational Fluid Mechanics*, edited by W. Kollmann, Hemisphere, NY, 1980, pp. 1–98.

[17]Maruszewski, J. P., and Amano, R. S., "Grid Generation and Its Application to Separated Flows," *Numerical Heat Transfer*, Vol. 21, Pt. B, 1992, pp. 183–197.

[18]VanDoormaal, J. P., and Raithby, G. D., "Enhancements of the SIMPLE Method for Predicting Incompressible Fluid Flows," *Numerical Heat Transfer*, Vol. 7, 1984, pp. 147–163.

[19]Hutchinson, B. R., Galpin, P. F., and Raithby, G. D., "Application of Additive Correction Multi-grid to the Coupled Fluid Flow Equations," *Numerical Heat Transfer*, Vol. 13, 1987, pp. 133–147.

[20]Peric, M., "Efficient Semi-Implicit Solving Algorithm for Nine-Diagonal Coefficient Matrix," *Numerical Heat Transfer*, Vol. 11, 1987, pp. 251–279.

[21]Dittus, F. W., and Boelter, M. K., Vol. 2, Univ. of California, Berkely, CA, 1930, p. 443.